Award Number: W81XWH-12-2-0075

TITLE: Lifetime Fluorescence and Raman Imaging for Detection of Wound Failure and Heterotopic Ossification

PRINCIPAL INVESTIGATOR: Grundfest, Warren S

CONTRACTING ORGANIZATION: The Regents of the University of California
Los Angeles, CA 90095

REPORT DATE: October 2013

TYPE OF REPORT: Annual

PREPARED FOR: U.S. Army Medical Research and Materiel Command
Fort Detrick, Maryland 21702-5012

REPORT DOCUMENTATION PAGE

Form Approved
OMB No. 0704-0188

1. REPORT DATE	**2. REPORT TYPE**	**3. DATES COVERED**
October 2013	Annual	15September2012-14September2013

4. TITLE AND SUBTITLE
Lifetime Fluorescence and Raman Imaging for Detection of Wound Failure and Heterotopic Ossification

5a. CONTRACT NUMBER

5b. GRANT NUMBER
W81XWH-12-2-0075

5c. PROGRAM ELEMENT NUMBER

6. AUTHOR(S)
Grundfest, Warren S

5d. PROJECT NUMBER

5e. TASK NUMBER

5f. WORK UNIT NUMBER

7. PERFORMING ORGANIZATION NAME(S) AND ADDRESS(ES)
The Regents of the University of California
Los Angeles, CA 90095

8. PERFORMING ORGANIZATION REPORT NUMBER

9. SPONSORING / MONITORING AGENCY NAME(S) AND ADDRESS(ES)
U.S. Army Medical Research and Materiel Command
Fort Detrick, Maryland 21702-5012

10. SPONSOR/MONITOR'S ACRONYM(S)

11. SPONSOR/MONITOR'S REPORT NUMBER(S)

12. DISTRIBUTION / AVAILABILITY STATEMENT
Approved for Public Release; Distribution Unlimited

13. SUPPLEMENTARY NOTES

14. ABSTRACT
The aim of this effort was to develop Raman and lifetime fluorescence imaging systems to assess failed wounds. The goal of these studies was to develop novel contrast mechanisms based on tissue pathologies which allow surgeons to identify wounds at risk for failure based on classifiers identified with these imaging systems. Our collaborative team built and characterized novel video rate imaging systems based on these technologies as a first step towards enabling early and accurate detection of failed wounds. Soldiers wounded in combat present with acute, traumatic wounds resulting from blasts, high speed projectiles, or intense burns. These injuries exhibit complicated healing responses and often fail to heal despite the application of advanced treatments [1-3]. Long term failure facilitates increased risk of infection and can lead to permanent disabilities or death. Current treatment methods include regular debridement of wounds, prophylactic antibiotics, special dressings, and wound drainage systems [1, 4]. Histopathologic testing of excised tissue from wounds for abnormal collagens, inflammatory cytokines, and phosphates have provided insight into the pathophysiology of wounds [1, 5, 6]. However, these are research techniques and due to their expense cannot be done with sufficient frequency to predict wound failure. We hypothesize that systems based on Raman and lifetime fluorescence imaging can give early warning of possible wound failure and provide additional information that will refine the treatment plan and improve wound healing prognoses.

15. SUBJECT TERMS- none provided

16. SECURITY CLASSIFICATION OF:			**17. LIMITATION OF ABSTRACT**	**18. NUMBER OF PAGES**	**19a. NAME OF RESPONSIBLE PERSON**
a. REPORT	**b. ABSTRACT**	**c. THIS PAGE**			USAMRMC
U	U	U	UU	15	**19b. TELEPHONE NUMBER** *(include area code)*

Lifetime Fluorescence and Raman Imaging for Detection of Wound Failure and Heterotopic Ossification

Introduction

The aim of this effort was to develop Raman and lifetime fluorescence imaging systems to assess failed wounds. The goal of these studies was to develop novel contrast mechanisms based on tissue pathologies which allow surgeons to identify wounds at risk for failure based on classifiers identified with these imaging systems. Our collaborative team built and characterized novel video rate imaging systems based on these technologies as a first step towards enabling early and accurate detection of failed wounds.

Soldiers wounded in combat present with acute, traumatic wounds resulting from blasts, high speed projectiles, or intense burns. These injuries exhibit complicated healing responses and often fail to heal despite the application of advanced treatments [1-3]. Long term failure facilitates increased risk of infection and can lead to permanent disabilities or death. Current treatment methods include regular debridement of wounds, prophylactic antibiotics, special dressings, and wound drainage systems [1, 4]. Histopathologic testing of excised tissue from wounds for abnormal collagens, inflammatory cytokines, and phosphates have provided insight into the pathophysiology of wounds [1, 5, 6]. However, these are research techniques and due to their expense cannot be done with sufficient frequency to predict wound failure. We hypothesize that systems based on Raman and lifetime fluorescence imaging can give early warning of possible wound failure and provide additional information that will refine the treatment plan and improve wound healing prognoses.

While all traumatic wounds express abnormal collagens in the first phase of the healing process, recent data suggests that these collagens dissipate throughout the later phases of normally healing wounds [1]. Conversely, failed wounds exhibit sustained, or increased abnormal collagen levels along with the presence of inflammatory cytokines [1]. An additional wound failure mechanism is the formation of Heterotopic Ossification (HO) [3, 7]. In these wounds collagen producing fibroblasts begin secreting phosphates which calcify quickly in the wound bed. If left untreated these constituents can coalesce into bone fragments causing pain in afflicted patients and often require deep debridement or amputation. Imaging systems based on both Raman and lifetime fluorescence technologies are both capable of detecting abnormal collagens and bone phosphates with high sensitivity and specificity while remaining robust to confounding factors that hinder *in vivo* imaging performance such as blood absorption and scattering. Previously these systems required point-by-point spectrometers with limited imaging capability and impractical illumination fluence.

Progress Summary:

This work focused primarily on the design, assembly, and construction of systems for detection of abnormal collagens and wound phosphates. The system work was divided into two separate thrusts: (1) fluorescence lifetime imaging, and (2) Raman imaging. The fluorescence lifetime imaging system was designed to detect abnormal collagens while the Raman system was designed to wound phosphates.

During these investigations we discovered new system architectures and data processing routines that have significantly improved contrast over what was available over what was presented in the original grant application. However, due to the complexity and stringent requirements of in vivo imaging we devoted significant time to refinement of system technology and have asked for a no cost extension to accommodate impending pre-clinical trial in rat models.

1. Raman Imaging

1.1. Traditional Raman imaging system Limitations

Traditional Raman imaging systems collect sampled spectra at each pixel position (**Figure 1a**). This is usually accomplished with a scanning sample stage, microscope/focusing objective, and dispersive spectrometer (often a monochromator) [8-11]. The illumination beam is focused onto target with the objective and the emission (Raman scattered light) is acquired by the spectrometer. This is done for each pixel and a 2D raster scan is typically required for image generation. Once a spectra for each pixel has been acquired methods such as peak power, power in the bucket, band area, and band area ratios are employed to transform spectral content into meaningful pixel values [8-11]. While this technique is a powerful scientific tool, it suffers from a number of weaknesses that have limited its use on patients.

Monochromators display significant off-axis aberrations due primarily to the entrance slit, dispersive element within the instrument, and collimating optics. Thus images formed from radiation passing through the entrance slit have poor resolution and aberrations in the very center of the FOV and progressively worse to unusable image quality as one observes radialy outward from the center. This limits most monochromator based systems to raster scanning only. In addition to significant off-axis aberrations, monochromators suffer from extremely low throughput on the order of - 30 dB. This is governed by the spectral resolution of the system. A narrow slit provides a larger solid angle of diffracted light which produces a broader spread of spectral components at the detector and thus higher spectral resolution. However, a narrow slit also reduces the available light at the detector thus resolution is only gained at the expense of signal and hence acquisition time. Furthermore, Raman signatures, such as the CH stretch are narrow (1 – 10 cm^{-1}) and necessitates the use of a narrow entrance slit .

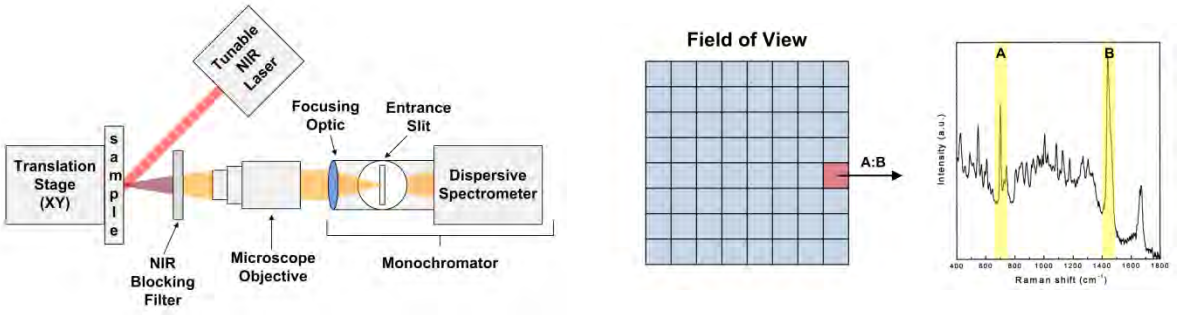

Figure 1: Methodology of Raman spectroscopic imaging. a.) Block diagram of typical Raman spectroscopic imaging system with grating spectrometer and translation stage. b.) Construction of an image from Raman spectra using band area ratios. Most Raman imaging systems compare the power of one particular peak to a reference peak. A false color map is assigned to a range of ratios and then the ratio map is displayed as an image.

One final point is the inefficiency of data use. Raman based imagers typically employ a band area ratio algorithm to generate images (Figure 1c). This equates to only a fraction of the total acquired spectrum utilized for image formation and represents a significant inefficiency in operation. The acquisition of unused data contributes significantly to impractically long acquisition times and is one of the primary hindrances to widespread clinical acceptance.

1.2. UCLA system

We have built the first Raman imaging system that acquires the full field in parallel by using tuned illumination and narrow band detection. A block diagram of this setup is displayed in Figure 2a. This architecture eliminates the monochromator and replaces it with a standard CCD focal plane array coupled to a very narrow, high throughput bandpass filter. The Raman imaging system tunes the illumination wavelength such that the expected Raman shifted wavelength (i.e. shifts for gliomas or HNSCC) falls into the filter pass band. Fast switching between wavelengths will allow high speed acquisition of the entire field of view for each shifted band of interest with extremely low illumination fluence.

2. Results

2.1. Microscopic results

To test the detection sensitivity and resolution of the system fragments of ground bone were sandwiched between layers of tissue analogues. A gray scale micrograph of the chosen fragment is displayed in Figure 2b where the bright spot is the bone fragment and the surrounding textured area is scotch tape. Scotch tape was selected as the mounting material because it has relatively good transmission at 611 nm and displays a low Raman emission at the 1090 cm-1 band. The bone fragment measures ~ 150 um in diameter and is ~ 10 um thick.

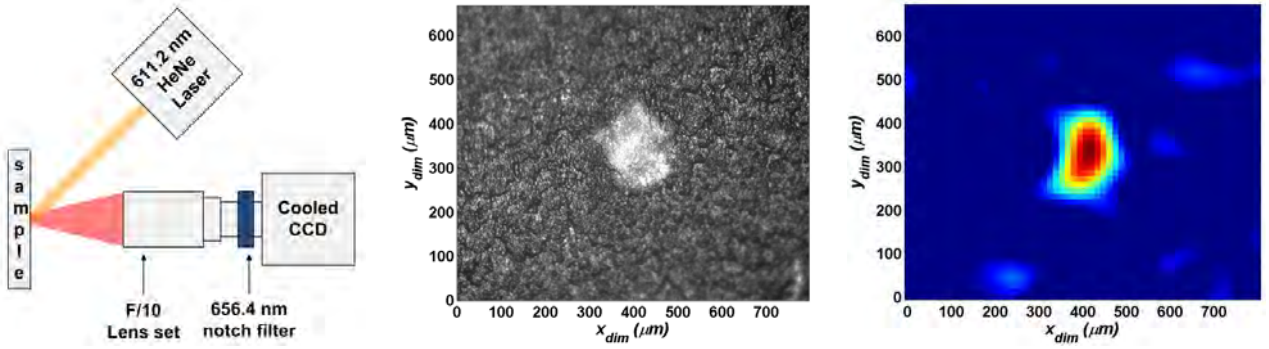

a.) b.) c.)

Figure 2: Video rate Raman imaging system and results. a.) Block diagram of Raman imaging system. b.) grayscale image of bone fragment on scotch tape. c.) Raman image of Bone fragment. Red corresponds to an increase in detected signal.

The full field of the Raman imaging system is displayed in Figure 2c where lighter shades of gray correspond to a higher level of received light at 657 nm (1090 cm-1 shift).The bone fragment is located at ~ 1 mm x 1 mm in the field and displays significant SNR. The light areas located on the left side of the image are the Raman signature of the scotch tape. Although clutter is visible in the image, the difference signal SNR between bone fragment and tape clutter is > 15 dB. From the inset image a total of 12 x 12 = 144 pixels were determined to lie within the boundaries of the target. This confirms that the Raman imaging system is limited by systemic parameters such as scattering coefficient, optics, and CCD/CMOS spatial sampling frequency and not by some intrinsic physical limit as are X-ray and MRI. From this data, a back projected pixel size (on target) of ~ 25 μm was computed; ~ 6x the resolution available to clinically deployed X-ray imaging systems. This is larger than the diffraction limited spot size of the system optics and confirms that our resolution is currently limited only by physical optics.

2.2. Wide field results

Following the resolution characterization, experiments were performed to determine system performance over a wide field of view and assess light scattering and absorption due to overlying muscle tissue. A bone chip measuring 2 mm x 8 mm from the same donor bone as the previous sample was selected and placed on the scotch tape backing used in the bone fragment experiments. The imaging system optics were then modified and the field of view expanded from 0.7 mm x 0.8 mm to ~ 7 mm x 8 mm. The illumination beam total power was limited to ~ 2 mW and with a ~ 1 cm diameter beam. This corresponds to ~ 25 μW/mm^2 and is orders of magnitude less than the accepted ANSI standards.

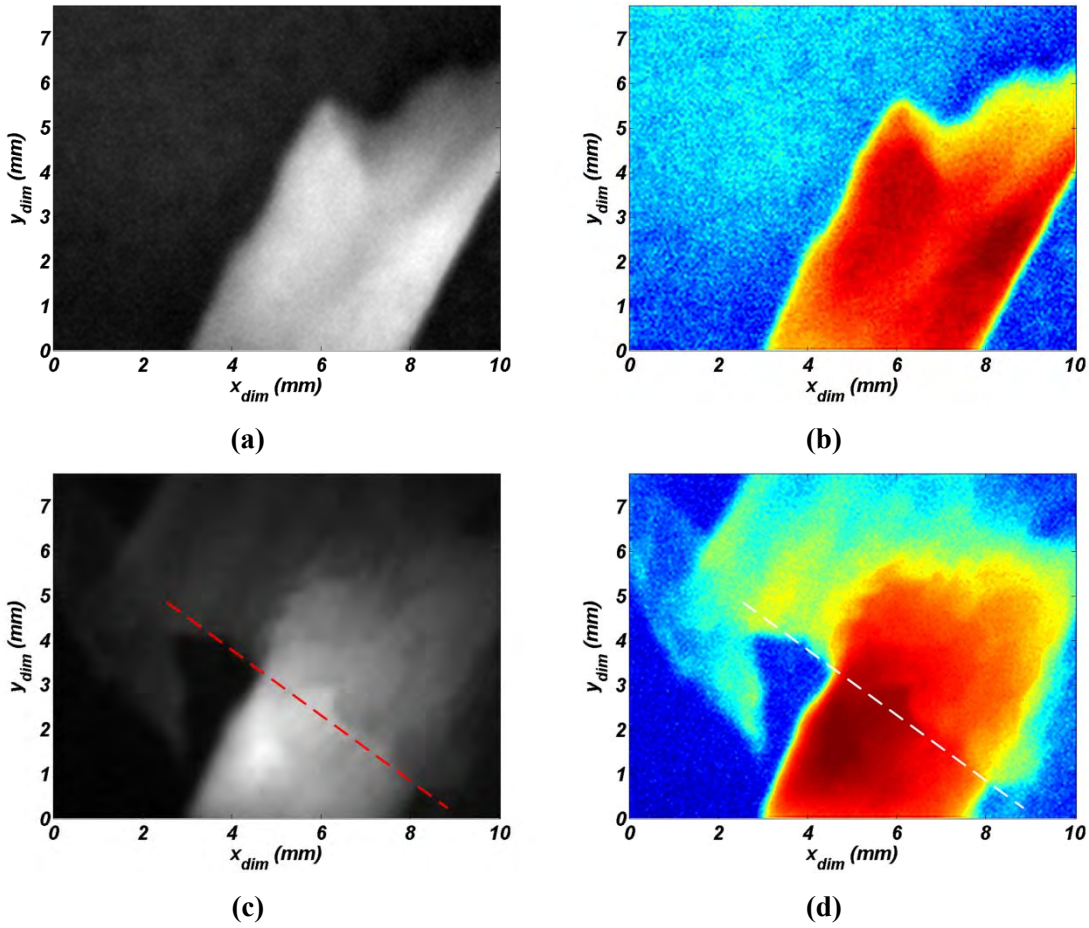

Figure 3: Wide field Raman imaging of bone. (a) Grayscale of exposed bone chip. (b) False color image of exposed bone chip. (c) Grayscale of bone chip obscured by 2 mm of muscle tissue. (d) False color of bone chip obscured by 2 mm of muscle tissue.

A grey scale image of the bone chip after a 5 minute exposure is displayed in Figure 3a and reflect the level of detected light at 657 nm emitted by the 1090 cm-1 shift. The false color mapping of this image is displayed in Figure 3b where red corresponds to higher intensity and blue lower. Edge definition is excellent and noise limited contrast is > 20 dB. A grayscale Raman image of the same bone chip with the top half obscured by ~ 1 mm thick muscle tissue is displayed in Figure 3c and false color map in Figure 3d. The muscle tissue covered the area in the image northeast of the dotted line. Light throughput is still sufficiently high for high contrast imaging with signal SNR still > 20 dB. While edge definition has suffer slightly from the diffuse scattering of the emitted 657 nm light through the overlying tissue this intensity map still displays contrast sufficient for calcification detection.

2.3. Image processing

Contrast enhancement and CCD readout noise suppression algorithms have been developed to extract the maximum contrast from each scene. The algorithms devloped to extract the contrast observed in Figure 2 and Figure 3 are discussed below.

Image processing was done with MATLAB's histogram equalization and 2D spatial convolution functions. The Raman scatter light is > 6 orders of magnitude below the applied illumination power and algorithms that convert low signal to useful contrast are

imperative to the development of a clinical system. The dim raw images generated by Raman imaging system typically have a significant number of pixels in the lower intensity regions of the intensity scale. The first step in the enhancement process is histogram equalization which spreads the distribution of the pixel intensities such that the cover the entire range afforded by the display system. This is achieved through a non-linear (sigmoidal) mapping of pixel values. While this brings out the features from the image, it accentuates high frequency noise. To decrease noise in the image, a 2D finite impulse response filter designed in the spatial frequency domain with the FFT was created to minimize enhancement noise while maintaining edge definition.

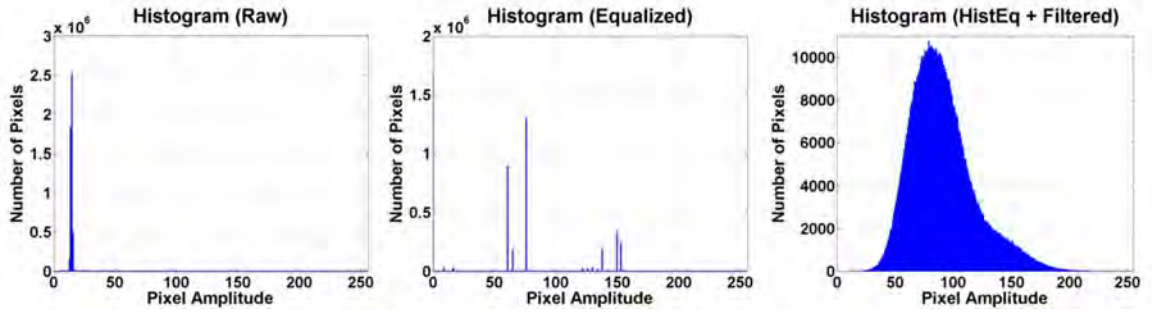

Figure 4: Implementation of histogram equalization and low-pass filtering a.) Histogram of the raw image. (b) histogram after equalization. (c) histogram following low-pass filter.

Figure 4a displays the pixel intensity histogram of a typical raw Raman image. A significant majority of the pixels display values in the lower 10% of the visible range. Histogram equalization intelligently redistributes these values such that they enhance contrast (Figure 4b). However, this process gives rise to high frequency noise as is evidence by the discrete nature of the histogram. Figure 4c displays the histogram of the final processed image following low pass filtering where the distribution of pixels has been smoothed out thus reducing high frequency noise.

3. Fluorescence Lifetime Imaging

After significant characterization and modeling work we have developed a new imaging modality which relies on difference in tissue fluorophore lifetime but does not attempt to extract actual lifetime values. We call this technology Functional Imaging using Fluorescence Decay Rate tuning (FIFDRT).

3.1. FIFDRT Inspiration: functional imaging using fluorescence lifetimes

The initial conception for FIFDRT was based on our earlier work in Fluorescence lifetime imaging (FLIM) and its ability to perform functional imaging [12-15]. FLIM is a technique where the auto-fluorescence of a sample is probed in both the wavelength and time domains by exciting the sample with a very short pulsed laser and detecting the auto-fluorescence lifetimes at a range of wavelengths. Lifetimes are dependent on the biochemical composition of the material and significant imaging contrast can be generated using maps of the measured decays. In many clutter dominated imaging fields (intraoperative imaging setting) time resolved fluorescence is superior to amplitude only fluorescence because the fluorophore lifetime of a tissue is almost completely invariant to

factors that would significantly degrade amplitude only measurements (i.e. absorption by blood, scattering by tissue surface geometry, and other confounding factors). Additionally, the fluorophore lifetimes are often strongly dependent on conditions related to physiological processes including oxygenation, pH, and temperature. This enables *in situ* functional imaging and potentially enables significant specificity in failed wound detection.

3.1.1. FLIM limitations

In principal, FLIM is an ideal modality for *in vivo* and intraoperative imaging due to its specificity, access to contrast mechanisms based on physiological processes, and mitigation of imaging confounders including geometry, non-uniform emission, and obscurants that can perturb the uniformity of illumination. However, FLIM has suffered from a number of practical constraints that have prevented successful clinical adoption [16, 17].

The primary restriction is the use of computationally intensive methods of lifetime extraction via orthogonal basis calculation (Laguerre polynomials) and curve fitting to identify fluorophore decay times and distributions [18-23]. In this methodology a picosecond pulsed laser illuminates the target and a gated spectrometer or wavelength filtered photomultiplier tube (PMT) samples the emission to create vectors of wavelength resolved decay rate measurements. The complexity of this data acquisition approach typically relegates this technique to point measurements. Further, although novel techniques have been employed to acquire data simultaneously [24-26] the picosecond pulse for lifetime extraction requires laser illumination that is difficult to use wide field due to coherence effects.

An additional problem with FLIM is that it requires solving an ill-posed inverse problem. There exists no robust, objective manner with which to choose the number of terms in expansion. Varying numbers of terms can produce fits that yield significant goodness of fit, but provide completely different interpretations of the results. Assuming tissue types *a priori* to limit the expected number of fluorophores helps to limit the polynomial form expanding to an unwieldy number of terms. However, the non-linear least squares based de-convolution and fitting algorithms are insufficiently fast to provide imaging contrast over a wide field at video rate. In contrast FIFDRT does not fit a model to the data and does not extract fluorophore lifetimes for every pixel in the image and requires only minimal computation, making it an ideal candidate for video rate imaging.

3.2. Functional imaging using fluorescence decay rate tuning (FIFDRT)

While challenges limiting clinical translation of FLIM are difficult to address, the potential sensitivity and specificity enabled by probing the functional status of tissue through fluorophore lifetime based contrast generation presents a novel and unique capability for in situ monitoring of tissue status. To take advantage of this contrast mechanism we developed a technique that seeks to generate contrast from differences in fluorophore lifetimes without the need to extract absolute lifetime values [27-30]. As detailed below this relaxes the requirements on the temporal profile of the illumination pulse, enabling us to replace the picosecond pulsed laser with nanosecond pulsed light emitting diodes (LEDs) which is a significant step towards clinical intraoperative use.

This technique is called functional imaging using fluorescence decay rate tuning (FIFDRT) and utilizes novel illumination pulse shaping to produce contrast between fluorophores of difference decay rates. The concept is detailed in Figure 5(a). A ~ 100 ns

long pulse with ~ 5 ns rise and fall times illuminates the target with long wave UV. A gated intensified charge coupled device (iCCD) is oriented to detect the fluorescence emission. Two images are acquired: (1) A fluorescence emission is acquired in the middle of the pulse. The fluorescence lifetimes of most tissue constituents of interest fall within the range of 1 ns to 10 ns [31-33]. An emission image, acquired starting at 50 ns following initial illumination can be considered as an accurate representation of steady state tissue auto fluorescence. This image is labeled the calibration image. (2) An image is acquired starting at ~ 1 ns after the fall of the illumination pulse. At this point (or any point following initial illumination decay) the areas of the field with the longer decay times are emitting more photons than the areas with the shorter photons. This image is the decay image. Upon acquisition of both frames the calibration image (image 1) is divided by the decay image (image 2) and the resulting pixel values are proportional to the aggregate fluorophore decay time of the illuminated area. These pixel values are referred to as relative lifetime values. The calibration image is subject to the same confounders as the decay image and thus removed from the final image.

This phenomenology has a number of key strengths that make it ideal for intraoperative imaging. First as discussed above, the lifetimes are not computed. Fitting is therefore not required making the technique computationally simple. Second, since lifetime identification is not necessary, pulse widths and fall times can be arbitrarily long, thus opening the possibility of LEDs driven by electronic pulses. Third, the difference in signal between the emission decay of two fluorophores is positively correlated with gate time. In other words, the longer the gate is open during the decay image, the larger the difference signal. Additionally, the signal to noise ratio (SNR) increases significantly due to increases in signal and decreased instrumentation variance and shot noise (noise processes arising from low numbers of detected photons). This is in stark contrast to FLIM where gates need to be short to accurately sample the decay time. A block diagram of the system phenomenology is given in Figure 1(b).

3.2.1. Pulse shaping and decay rate tuning

Through signal modeling efforts (Figure 1(c),(d)) we have discovered that if a multi-fluorophore system is pumped with linearly decaying pulse as opposed to its natural exponential response, the difference in detected emission in the decay image is increased. In practice, a finite optical pulse with a well-defined linearly decaying slope is difficult to accomplish due to the intrinsic resistor-capacitor (RC) time constant arising from the physical size of the LED. However, if a stub as added to the output of the driving circuit it acts as a delay line loop to deplete the trailing edge charge in the circuit. This combination of the reflected pulse from the stub line and the pulse transmitted across the junction between the stub and the transmission line collectively forms the final linearly decaying impulse response.

3.2.2. System implementation

Our FIFDRT system implementation utilizes an illuminated subsystem consisting of 6 UV-LEDs arranged in a circular formation (375nm, Thorlabs) each rated at 2 mW usable optical power. The LED circuit was driven by a pulse generator (AVR-E2-C, Avtech) at 50 volts with a current of ~1 Amp. The LED circuit operated at an average optical power of ~4.5 μ W with peak power of < 3mW at 0.02% duty cycle. A low duty cycle ensured thermal stability of the LED array and long operational time under these settings. The LED illumination characteristics (i.e. pulse width and peak intensity) were measured using a fast

photomultiplier tube and confirmed to be linear with minimal ringing following the decay. An intensified CCD camera (DH 734 18U-03, iStar intensified CCD camera, Andor technology) captured images of the fluorescence calibration and decay images.

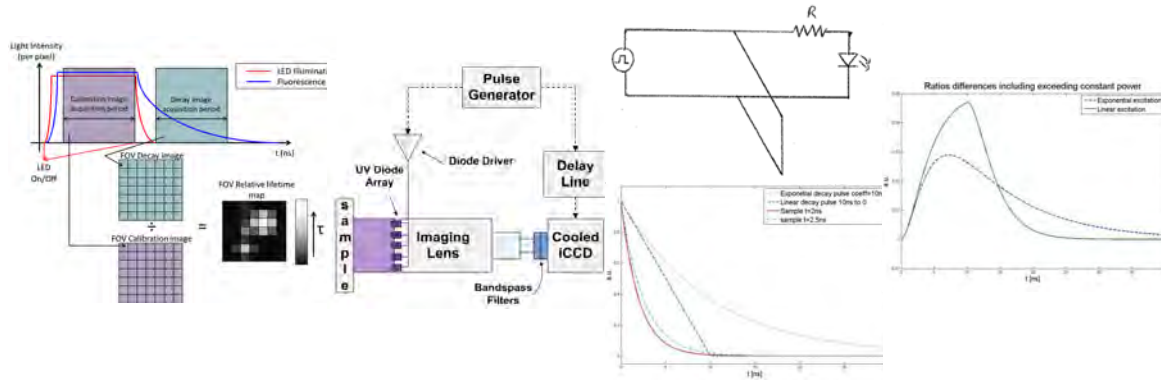

(a) **(b)** **(c)** **(d)**

Figure 5: Novel Functional imaging using fluorescence decay rate tuning (FIFDRT). (a) Image generation algorithm. (b) Block diagram of system. (c) Stub tuned driving circuit and associated linear decay curve (d) Contrast differences between imaging with exponentialy decaying illumination and linearly decaying illumination.

The gated, iCCD was operated with a gate width of ~ 10 ns and is capable of gate widths as low as 2 ns. Gate timing can also be controlled with a temporal resolution of 0.1 ps. The duration of the pulse was ~ 100 ns with a repetition rate of 10 kHz. The pulse generator triggered the gated iCCD to synchronize the optical illumination with the image acquisition. A motorized filter wheel (Edmund Optics, RS-232 Motorized Filter Wheel) containing ten bandpass filters (Semrock Fluorescence filters) centered at: 407nm, 434 nm, 465 nm, 494 nm, 520 nm, 542 nm, 572 nm, 605 nm, 652 nm, 676 nm with ~20 nm bandwidth was used to obtain spectral information. A UV rejection filter (Edmund Optics, 400 nm longpass filter) was used in conjunction with the bandpass filters to further reject reflected UV illumination. The fluorophore lifetimes of many tissue constituents (i.e. Elastins and collagens) display a strong dependence on detection wavelength [27-30] thus some wavelengths may offer more discriminatory power than others. The optimal wavelength for detection of abnormal collagens in an in vivo setting is still unknown thus the entire visible band was probed.

Overall, this system achieves functional imaging by assessing differences in fluorophore decay times and then tunes the decay rates to maximize contrast. The simplicity and intrinsic sensitivity of the technology enables real time imaging of large fields and is ideally suited to intraoperative imaging. Current image acquisition times take seconds and image acquisition time (currently performed offline) takes milliseconds.

Key Research Accomplishments:

- Design, characterization and verification of a Raman imaging system
- Design, characterization and verification of an FIFDRT based imaging system
- Successful

Reportable Outcomes:

Four conference proceedings have been published and one patent has been filed. 3 graduate students and 3 undergraduates are currently working on the project.

Publications:

[1] W. S. Grundfest and Z. D. Taylor, "Biophotonics at UCLA," in *Univeristy of California Biophotonics Alliance (UCBA)*, San Franciso, CA, 2012.

[2] A. Papour, Z. D. Taylor, W. Yong, M. S. John, O. Stafsudd, and W. S. Grundfest, "Multi-Spectral Fluorescence Lifetime Contrast Imaging for Brain Cancer Detection," in *Biomedical Engineering Society (BMES) Annual Meeting*, Atlanta, GA, 2012.

[3] A. J. Sherman, A. Papour, W. S. Grundfest, Z. D. Taylor, and O. M. Stafsudd, "Normalized fluorescence lifetime imaging for tumor identification and margin delineation," in *SPIE Advanced Biomedical and Clinical Diagnostic Systems XI*, San Francisco, 2013.

[4] Z. D. Taylor, A. Papour, O. M. Stafsudd, and W. S. Grundfest, Eds., *Lasers in Medicine* (Medical Devices. Wiley, 2012, p.^pp. Pages.

Patents:

[1] W. S. Grundfest, O. M. Stafsudd, P.-C. Jiang, A. Papour, and Z. D. Taylor, "Time-Resolved Fluorescence Imaging without Lifetime Fitting and Illumination Pulsed Shaping for Fluorescence Lifetime Imaging Microscopy (Film) Enhancement," United States of America Patent 61/605844, 2012.

Future Plans:

For the upcoming year we plan to accomplish the following tasks:

- Continue system refinement
- Pre-clinical animal imaging work

Conclusion:

Significant work has been achieved in imaging and detection of tissue constituents correlated with failed wounds. We intend to continue this work with extensive preclinical animal imaging

References.

[1] N. J. Crane, T. S. Brown, K. N. Evans, J. S. Hawksworth, S. Hussey, D. K. Tadaki*, et al.*, "Monitoring the healing of combat wounds using Raman spectroscopic mapping," *Wound Repair and Regeneration,* vol. 18, pp. 409-416, 2010.

[2] A. Medina, P. G. Scott, A. Ghahary, and E. E. Tredget, "Pathophysiology of Chronic Nonhealing Wounds," *Journal of Burn Care & Research,* vol. 26, pp. 306-319, 2005.

[3] B. K. Potter, T. C. Burns, A. P. Lacap, R. R. Granville, and D. A. Gajewski, "Heterotopic Ossification Following Traumatic and Combat-Related Amputations," *Journal Of Bone & Joint Surgery,* vol. 89a, 2007.

[4] P. G. Bowler, "Wound pathophysiology, infection and therapeutic options," *Ann Med,* vol. Vol. 34, pp. 419-427, 202.

[5] M. C. Robson, "Disturbances of Wound Healing," *Annals of Emergency Medicine,* vol. 17, pp. 1274 - 1278, 1988.

[6] J. Li, J. Chen, and R. Kirsner, "Pathophysiology of acute wound healing," *Clinics in Dermatology,* vol. 25, pp. 9–18, 2007.

[7] D. E. Garland, C. E. Blum, and R. L. Waters, "Periarticular Heterotopic Ossification in Head-Injured Adults," *J Bone Joint Surg Am.,* vol. 62-A, pp. 1143-1146, 1980.

[8] K. P. J. Williams, G. D. Pitt, B. J. E. Smith, A. Whitley, D. N. Batchelder, and I. P. Hayward, "Use of a rapid scanning stigmatic Raman imaging spectrograph in the industrial environment," *Journal of Raman Spectroscopy,* vol. 25, pp. 131-138, 1994.

[9] N. Hayazawa, "Near-field Raman imaging of organic molecules by an apertureless metallic probe scanning optical microscope," *J. Chem. Phys.,* vol. 117, p. 1296, 2002.

[10] R. Salzer, G. Steiner, H. H. Mantsch, J. Mansfield, and E. N. Lewis, "Infrared and Raman imaging of biological and biomimetic samples," *Fresenius' Journal of Analytical Chemistry,* vol. 366, pp. 712-726, 2000.

[11] P. J. Treado, I. W. Levin, and E. N. Lewis, "High-Fidelity Raman Imaging Spectrometry: A Rapid Method Using an Acousto-optic Tunable Filter," *Appl. Spectrosc.,* vol. 46, pp. 1211-1216, 1992.

[12] K. Dowling, S. C. W. Hyde, J. C. Dainty, P. M. W. French, and J. D. Hares, "2-D fluorescence lifetime imaging using a time-gated image intensifier," *Optics Communications,* vol. 135, pp. 27-31, 2/1/ 1997.

[13] V. Ntziachristos and B. Chance, "Breast imaging technology: Probing physiology and molecular function using optical imaging - applications to breast cancer," *Breast Cancer Res,* vol. 3, pp. 41 - 46, 2001.

[14] P. I. H. Bastiaens and A. Squire, "Fluorescence lifetime imaging microscopy: spatial resolution of biochemical processes in the cell," *Trends in Cell Biology,* vol. 9, pp. 48-52, 2/1/ 1999.

[15] P. J. Tadrous, "Methods for imaging the structure and function of living tissues and cells: 2. Fluorescence lifetime imaging," *The Journal of Pathology,* vol. 191, pp. 229-234, 2000.
[16] S. Shrestha, B. E. Applegate, J. Park, X. Xiao, P. Pande, and J. A. Jo, "High-speed multispectral fluorescence lifetime imaging implementation for in vivo applications," *Optics Letters,* vol. 35, pp. 2558-2560, 2010/08/01 2010.
[17] S. A. Hilderbrand and R. Weissleder, "Near-infrared fluorescence: application to in vivo molecular imaging," *Current Opinion in Chemical Biology,* vol. 14, pp. 71-79, 2// 2010.
[18] L. Marcu, J. A. Jo, P. V. Butte, W. H. Yong, B. K. Pikul, K. L. Black*, et al.*, "Fluorescence Lifetime Spectroscopy of Glioblastoma Multiforme¶," *Photochemistry and Photobiology,* vol. 80, pp. 98-103, 2004.
[19] P. V. Butte, A. N. Mamelak, M. Nuno, S. I. Bannykh, K. L. Black, and L. Marcu, "Fluorescence lifetime spectroscopy for guided therapy of brain tumors," *NeuroImage,* vol. 54, pp. S125-S135, 2011.
[20] P. V. Butte, B. K. Pikul, A. Hever, W. H. Yong, K. L. Black, and L. Marcu, "Diagnosis of meningioma by time-resolved fluorescence spectroscopy," *Journal of Biomedical Optics,* vol. 10, pp. 064026-9, 2005.
[21] Q. Fang, T. Papaioannou, J. A. Jo, R. Vaitha, K. Shastry, and L. Marcu, "Time-domain laser-induced fluorescence spectroscopy apparatus for clinical diagnostics," vol. 75, pp. 151-162, 2004.
[22] J. D. Meier, H. Xie, Y. Sun, Y. Sun, N. Hatami, B. Poirier*, et al.*, "Time-resolved laser-induced fluorescence spectroscopy as a diagnostic instrument in head and neck carcinoma," *Otolaryngology - Head and Neck Surgery,* vol. 142, pp. 838-844, 2010.
[23] L. Marcu, "Fluorescence lifetime in cardiovascular diagnostics," *Journal of Biomedical Optics,* vol. 15, pp. 011106-10, 2010.
[24] J. Requejo-Isidro, J. McGinty, I. Munro, D. S. Elson, N. P. Galletly, M. J. Lever*, et al.*, "High-speed wide-field time-gated endoscopic fluorescence-lifetimeimaging," *Optics Letters,* vol. 29, pp. 2249-2251, 2004/10/01 2004.
[25] M. G. L. Gustafsson, "Nonlinear structured-illumination microscopy: Wide-field fluorescence imaging with theoretically unlimited resolution," *Proceedings of the National Academy of Sciences of the United States of America,* vol. 102, pp. 13081-13086, September 13, 2005 2005.
[26] E. van Munster and T. J. Gadella, "Fluorescence Lifetime Imaging Microscopy (FLIM)," in *Microscopy Techniques*. vol. 95, J. Rietdorf, Ed., ed: Springer Berlin Heidelberg, 2005, pp. 143-175.
[27] A. J. Sherman, A. Papour, W. S. Grundfest, Z. D. Taylor, and O. M. Stafsudd, "Normalized fluorescence lifetime imaging for tumor identification and margin delineation," in *SPIE Advanced Biomedical and Clinical Diagnostic Systems XI*, San Francisco, 2013.
[28] Z. D. Taylor, A. Papour, O. M. Stafsudd, and W. S. Grundfest, Eds., *Lasers in Medicine* (Medical Devices. Wiley, 2012, p.^pp. Pages.
[29] W. S. Grundfest, O. M. Stafsudd, P.-C. Jiang, A. Papour, and Z. D. Taylor, "Time-Resolved Fluorescence Imaging without Lifetime Fitting and Illumination

Pulsed Shaping for Fluorescence Lifetime Imaging Microscopy (Film) Enhancement," United States of America Patent 61/605844, 2012.

[30] A. Papour, Z. D. Taylor, W. Yong, M. S. John, O. Stafsudd, and W. S. Grundfest, "Multi-Spectral Fluorescence Lifetime Contrast Imaging for Brain Cancer Detection," in *Biomedical Engineering Society (BMES) Annual Meeting*, Atlanta, GA, 2012.

[31] R. Cubeddu, G. Canti, A. Pifferi, P. Taroni, and G. Valentini, "Fluorescence Lifetime Imaging of Experimental Tumors in Hematoporphyrin Derivative-Sensitized Mice," *Photochemistry and Photobiology,* vol. 66, pp. 229-236, 1997.

[32] P. Provenzano, K. Eliceiri, and P. Keely, "Multiphoton microscopy and fluorescence lifetime imaging microscopy (FLIM) to monitor metastasis and the tumor microenvironment," *Clinical & Experimental Metastasis,* vol. 26, pp. 357-370, 2009/04/01 2009.

[33] P. S. Considine, "Effects of Coherence on Imaging Systems," *Journal of the Optical Society of America,* vol. 56, pp. 1001-1007, 1966/08/01 1966.